Twin applications of highly selective Cu^{2+} fluorescent Chemosensor and Cytotoxicity of 2-(2-phenylhydrazono)-1H-indene-1,3(2H)-dione and 2-(2-(4-methoxyphenyl)hydrazono)-1H-indene-1,3(2H)-dione: Molecular docking and DFT Studies

Annamalai Subhasri[a], Chinnadurai Anbuselvan[a]* and Nagarajen Rajendraprasad[b]

[a]*Department of Chemistry, Annamalai University, Annamalainagar − 608 002, India.*

[b]*Department of Biochemistry and Biotechnology, Annamalai University, Annamalai Nagar− 608 002, India.*

*Corresponding author: Address

C. Anbuselvan

Assistant professor,

Department of Chemistry

Annamalai University

Annamalainagar 608 002

E-mail: *cas_amu@yahoo.co.in*

A fluorescent chemosensor based on 2-(2-phenylhydrazono)-1*H*-indene-1,3(2*H*)-dione **(1)** and 2-(2-(4-methoxyphenyl)hydrazono)-1*H*-indene-1,3(2*H*)-dione **(2)** with high sensitivity and selectivity toward paramagnetic Cu^{2+} was developed over other cations. The Cu^{2+}-induced fluorescence turn–on mechanism was revealed to be mediated by intramolecular charge transfer from the ligand to the metal. The compounds were characterized by UV-Vis, FT-IR, ^{1}H and ^{13}C NMR techniques, scanning electron microscopy (SEM), energy dispersive spectroscopy (EDS), elemental color mapping and fluorescence spectroscopy. Morphology changes of compound **(1)** and **(2)** to complex with Cu^{2+} are also investigated by SEM. EDS analysis expose the occurrence of copper in complexes. Elemental color mapping are also support the copper present in the complexes of corresponding compound **(1)** and **(2)**. The metal sensing (Chemosensing) properties of compound **(1)** and **(2)** are also examined by fluorescence spectroscopy. The sensor shows excellent selectivity with fluorescence enhancement to copper over other cations in ethanolic solution. Chelating functionality of compound **(1)** and **(2)** were evaluated for their inhibitory properties against various human cancer proteins like 4LRH, 4EKD, 4GIW and 4L9K using online docking Server. From the cytotoxicity study, the ability of these compounds (**1**) and (**2**) to inhibit the growth of KB cell lines. A combined experimental and theoretical studies were carried out on the molecular structure using density functional methods (B3LYP) invoking 6-31G basis set. The density functional theory (DFT) calculation was carried out for both compounds. Energy of the highest occupied molecular (HOMO) orbital and lowest unoccupied (LUMO) molecular orbital have been predicted.

Introduction

An improvement of expedient selective fluorescent chemosensors for the finding of important species, such as certain transition, non-transition metal ions and anions is of current interest because of a variety of biological and environmental evils which cause serious problems for human health and ecology. Chemical sensing refers to the continuous monitoring of the presence of chemical species.[1-5] Many disciplines need sensing systems, including chemistry, biology, clinical biology and environmental science.

Some money consuming and complicated methods, such as atomic absorption[6] and Inductively coupled plasma, atomic emission spectroscopy,[7] for the detection of toxic metal ions have been employed to detect. Compared with all of these sophisticated experimental methods, fluorescent chemosensors are often used to detect many ions due to their simplicity and sensitivity, low cost, high selectivity and instantaneous response.[8, 9] The classical design of a fluorescent indicator includes two moieties, a receptor responsible for the molecular recognition of the analyte and a fluorophore responsible of signaling the recognition event. Copper is a one of the vital element in the human body, a co-factor in a variety of enzymes and copper-based pigments. Despite its significant roles in organisms, the accumulation of excess amounts of copper ions or their misregulation can cause a series of cruel diseases. It is believed that the disruption of copper homeostasis is implicated to some neurodegenerative disorders like Alzheimer's and Parkinson's diseases.[10, 11] The past years have seen increasing interest in design and synthesis of fluorescent chemosensors with a Cu^{2+} induced "turn-on" fluorescence signal. However, only few sensors are presently obtainable because the implementation of sensing probes in functional devices without the loss of sensitivity is still very challenging.[12] Lu *et al.*

have reported a functional oligonucleotide-based "turn-on" fluorescent probe for detection of Cu^{2+} in aqueous solution with satisfying sensitivity and selectivity.[13] Swamy *et al,* have proposed a monoboronic acid-conjugated rhodamine based probe for Cu^{2+} with a reversible fluorescence "turn-on" response and high selectivity, and they successfully applied it to image Cu^{2+} in living cells and organisms.[14]

Aryl hydrazones are significant classes of compounds which have long fascinated awareness, owing to their considerable biological and pharmacological properties, such as antibacterial, antiviral, antineoplastic, and antimalarial behavior.[15] The resonance-assisted hydrogen bond systems engage a synergistic reinforcement of hydrogen bonds by delocalization of a p-conjugated chain connecting donor and acceptor atoms, they have been applied for the activation of a carbon in α-position to a carbonyl, induced enolization in keto–enol tautomerism, controlled crystal packing, formation of H-bonds in functional molecular materials, activation of dinitriles towards formation of amidines, carboxamides and iminoesters, etc. while special interest should be paid to the nature of the strong intramolecular O…H−N resonance-assisted hydrogen bond and its influence on the enol-azo $\rightleftharpoons$ hydrazone transformation.[16–19] The rich tautomerism and isomerism of aryl hydrazones together with the intramolecular resonance assisted hydrogen bond system can be applied for regulation of tautomerization-isomerization, activation of the carbon in α-position to a carbonyl, antiferroelectric paraelectric transition, regioselective activation of dinitriles, catalysis, ligand liberation, etc.[20] In some cases hydrogen bonding acts as an active site for initiation of chemical reaction. These results led to the observation that the system exists in a conformation with a preferred orientation where the stereoelectronic constraints and the stabilizing effect of hydrogen bonding are competing.

In this article, we demonstrate the use of compound **(1)** and **(2)** as a highly efficient fluorescent chemosensor for Cu^{2+}. In terms of sensitivity concerns, chemosensors exhibiting fluorescence enhancement (fluorescence "turn on") upon Cu^{2+} ion complexation are favoured. Among these detection approaches for the Cu^{2+} ion, fluorescence spectroscopy was used because of its high sensitivity, high selectivity and low cost. Our sensor shows simple and good selectivity compared to the recently developed Cu^{2+} sensors [21–28] attributed to the very high association constants for the binding of Cu^{2+}.

Experimental

All of the solvents were analytical reagent grade. The homogeneity of the compounds was monitored by ascending thin layer chromatography (TLC) on silica gel-G (Merck) coated aluminum plates, visualized by iodine vapor and UV light. IR spectra were recorded on an Avatar Nicholet FT-IR spectrophotometer (range 4000–400 cm^{-1}) in KBr pellets (λ_{max} in cm^{-1}). ^1H and ^{13}C NMR spectra for analytical purpose were recorded in $CDCl_3$ on a Bruker instrument at 400 MHz, chemical shifts are expressed in δ-scale downfield from TMS as an internal standard. SEM analysis was performed for surface morphology of compound (**1**), compound (**2**) and corresponding complexes with Cu^{2+}, on platinum coated samples using a JEOL JSM-5610 SEM. EDS analysis was performed on using a JEOL JSM-5610 SEM equipped with EDS. UV–vis spectra were recorded on a SHIMADZU UV-1650PC spectrophotometer by dissolving the sample in spectral grade ethanol using a 1 cm path length quartz cell. A Perkin Elmer LS 55 fluorescence spectrometer was employed to record the fluorescence (FL) spectra at room temperature. The choice of excitation wavelengths was based on the absorbance spectral characteristics.

Preparation of Compounds

Compounds were prepared by the general procedure (Scheme 1) which anilines (0.5 mmol) were dissolved separately in 1 N HCl (25 cm^3) at 0-5 °C temperature and in each case cooled aqueous solution (10 cm^3) of $NaNO_2$ (0.40 g) was added drop wise with stirring followed by the addition of indene-1,3-dione (0.73 g, 0.5 mmol) and sodium acetate (5.0 g) dissolved in water (30 cm^3). Corresponding mixtures were further stirred for 4 h at room temperature (25 °C). Solids thus obtained were filtered and washed several times with water followed by ethanol and then dried in vacuum. The crude products were recrystallized in ethanol. Compounds **(1)** and **(2)** were purified by column chromatography by using benzene as eluent. Yield and melting points of the derived compounds are mention below.

Computational details

Theoretical investigations on Compounds **(1)** and **(2)** , Compounds **(1)** and **(2)** -Cu^{2+} by the GAUSSIAN 03W program package,[29] invoking gradient geometry optimization at the B3LYP level and the LANL2DZ effective core potential was used for all of the atoms.[30] Initial geometry generated from standard geometrical parameters was minimized without any constraint in the potential energy surface at ab initio adopting the standard 6-31G basis set.

Results and discussion

2-(2-phenyl)hydrazono)-2H-indene-1,3-dione **(1)**

yellow solid, yield: 92 %, m. p. 197 °C; IR (KBr, cm^{-1}) 3421, 3083, 3043, 3018, 2922, 2850, 1718, 1664, 1539 (**Fig. S1**); ^{1}H NMR (400 MHz, CDCl$_3$) (δ): 7.22-7.96 (aromatic protons),

13.48 (s, NH) **(Fig. S3)**; ^{13}C NMR (125 MHz, CDCl$_3$) (δ) 116.3, 122.9, 123.2, 125.7, 126.3, 127.3, 128.3, 129.7, 135.0, 135.3, 140.6, 141.0, 144.1, 186.1, 188.0 **(Fig. S4).**

2-(2-(4-methoxyphenyl)hydrazono)-2H-indene-1,3-dione **(2)**

Orange solid, yield: 87 %, m. p. 190 °C; IR (KBr, cm^{-1}) 3431, 3154, 2962, 2923, 2851, 1711, 1671, 1592 **(Fig. S2)**; ^{1}H NMR (400 MHz, CDCl$_3$) (δ): 3.85 (s, OCH$_3$), 6.95-7.93 (aromatic protons), 13.63 (s, NH) **(Fig. S5)**; ^{13}C NMR (125 MHz, CDCl$_3$) (δ) 55.7, 115.0, 117.8, 122.6, 123.0, 129.9, 134.5, 134.7, 135.0, 138.7, 140.4, 158.5, 186.4, 188.9 **(Fig. S6).**

The arylhydrazones of 2-(2-phenyl)hydrazono)-2H-indene-1,3-dione **(1)** and 2-(2-(4-methoxyphenyl)hydrazono)-2H-indene-1,3-dione **(2)** have been synthesized and their IR spectra of 1 and 2 show $\nu_{(NH)}$ vibration at 3421-3431 cm^{-1}, while $\nu_{(C=O)}$, $\nu_{(C=O...H)}$ and $\nu_{(C=N)}$ are observed at 1718–1711, 1664–1671 and 1539–1592 cm^{-1} respectively **(Fig. S1 and S2)**. These bands can be related to the intramolecular hydrogen bonded hydrazone fragment. This conclusion was further supported by the ^{1}H and ^{13}C NMR spectrum, the 1H NMR spectra of **(1)** and **(2)** show signals at 13.48-13.63 ppm which can be assigned to the proton of the NH moiety adjacent to aryl unit. In compound **2** the methoxy proton appeared at 3.85 ppm. In compound **1** and **2** the aromatic proton signals appear in the downfield region of 6.95–7.96 ppm with the expected splitting patterns. Carbonyl sp^2 carbon atoms appear as separate signals in the low field region of about 186 and 188 ppm for C-**(1)** and C-**(2)**, respectively. Strong intramolecular N–H……O–C hydrogen bonding deshields C-**(1)** with respect to C-**(2)** to the extent of ca. 2 ppm.

Solvatochromism

The absorbtion spectra of compounds (1) and (2) were measured in various solvents of different polarity and shown in figure S7A and S7B . The longest wavelength absorption band

has been assigned to $n - \pi^*$ transition. This band is associated with a charge transfer from N-H group to the carbonyl oxygen (C=O) due to intramolecular hydrogen bonding between them. This intramolecular hydrogen bond is responsible for the stabilization of the charge transfer band. A shoulder at shorter wavelength around 480 nm is due to $\pi - \pi^*$ transition. In particular for hydazone derivatives charge transfer between a donor part, N–H (D) and an acceptor part, indene1,3-dione (C=O), has been considered. Both donor and acceptor appear to be localized in the quasi aromatic rings (Fig. 9) containing the intramolecular hydrogen bonds. So, these hydrogen-bonded quasi-aromatic rings contribute to the stabilization of the charge transfer band.

The emission spectra of compounds (**1**) and (**2**) were studied in various solvents. The results are summarized in Table S1 and the spectrum of compound (**1**) and (**2**) in various solvents are depicted in Fig. S8A and S8B. The compound (**1**) shows two emission bands: one band occurs at around 460 nm and another band occurs at around 480 nm. It is assumed that the longer one for Charge Transfer (CT) and the shorter one for Local Excitation (LE) [31,32,33]. In both the compounds the Photoinduced Electron Transfer(PET) from donor to the acceptor produces a low lying anomalous CT state which leads to new longer wavelength fluorescence. Emission maximum of the both the states found to be independent of the excitation Wavelength. In protic solvents, protonation of the fluorophore increases oxidation state of donor group which results in the LE of fluorescence only. The LE state is more enhanced in intensity when compared to CT state due to the increased charge density on nitrogen.

Similarly compound (**2**) has LE at 485 nm and CT band at 515 nm. The variations in solvatochromic properties of compounds (**1**) and (**2**) depend on the substitution pattern. The red shift of the emission maximum increases in -OCH$_3$ substituted compound (**2**) when compared to compound (**1**). This observation reveals the significant influence of H-bonding on the

solvatochromic properties, presumably as a result of the stabilization of the negative charge at the carbonyl oxygen atoms during solvent relaxation.

To better understand the solvent polarity effect, the Lippert–Mataga relation was applied. This relation has been widely used to correlate the energy difference between absorption (v_a) and emission (v_f), also known as Stokes shift, with solvent polarity represented by Δf. This relation was given in equation. (1). It involves both the dielectric constant and the refractive index (n) of the solvents.[34, 35]

$$v_a - v_f = \frac{2(\mu_E - \mu_G)^2}{hca^3} \Delta f + \text{constant} \quad \text{.........................} \quad (1)$$

In equation (1), v_a and v_f are the wavenumbers (cm^{-1}) corresponding to the absorption and the emission, respectively, h is Planck's constant, c is the speed of light, and a is the radius of the solvent cavity in which the fluorophore resides. For an elongated shape of the molecule, a is usually estimated as 40% of its longest axis.[36] The term (Δf) involving ε and n is called the orientation polarizability, which only accounts for the spectral shifts due to the reorientation of the solvent molecules. Therefore, the Lippert–Mataga relation is based on the assumption that the energy difference is only proportional to the solvent orientation polarizability (known as the general solvent effect). Inability of Stokes' shift to increase linearly with Δf usually implies that specific solvent effects are involved.

$$\Delta f = \frac{\varepsilon - 1}{2\varepsilon + 1} - \frac{n^2 - 1}{2n^2 + 1} \quad \text{.........................} \quad (2)$$

(Fig. S9). showed the Lippert–Mataga plots of compounds **(1)** and **(2)** in 13 organic solvents. The estimation from the Lippert–Mataga equation is based on the assumption that the photophysical properties of compounds **(1)** and **(2)** can be described by the theory of general solvent effect; hence, it may not hold if specific solvent effects are involved. Stokes shift slightly increases with increasing polarity of the solvent (as it is expected based on the CT character of the excited state) and does not follow a linear dependence on f(ε, n) in all solvents used, ie., solvent specific interactions observed. The linear variation of the Stokes shift with ET (30) (with solvent polarity parameter) has been shown in Fig. S10. The compounds **(1)** and **(2)** exhibit an slightly increase or no increase of Stokes shift from non-polar to polar aprotic solvents mainly due to the combined effect of increasing the polarity of the medium and intramolecular charge transfer (CT) state and it confirmed that solvent polarity cannot affect the stoke shift of compounds **(1)** and **(2)**. The v_A– v_F value is unusually small in hexane and remarkably deviates from the linear correlation. This deviation is particularly connected with decrease of λ_F in hexane and indicates different charge redistribution of the excited state of 1 than in other solvents. This suggested that the solvent polarity might not be the only factor affecting the spectral shifts. Specific solvent effects including hydrogen bonding, acid–base chemistry, and charge transfer interactions can also result in nonlinear Lippert–Mataga plots.

Chemosensor

The response of compounds **(1)** and **(2)** to various metal ions were investigated in aqueous buffer. It displays a very distinctive selectivity for copper ions, as observed by the fluorescence spectroscopy. When compounds **(1)** and **(2)** were treated with various metal ions, such as Cd^{2+}, Ni^{2+} , Pb^{2+}, Zn^{2+}, Ag^+, Hg^{2+}, Cu^{2+}, Mn^{2+}, Fe^{2+}, Cr^{3+}, K^+, Fe^{2+}, Fe^{3+}, $Al^{3+}$and Co^{2+} in the buffer, complete fluorescence enhancement was observed only for Cu^{2+} ions not for other

metal ions. The fluorescence responses of the sensors (1) and (2) to various cations and its selectivity for Cu^{2+} were illustrated in Fig. 6A and 7A. The fluoroionophoric behavior of sensors (1) and (2) were investigated in ethanol–water (1: 1, v/v) solution [sensor (1) and (2)] = 1 and 2 μM, $[Cu^{2+}]$ = 1 μM, as expected, sensors (1) and (2) showed a weak fluorescence in aqueous solution. Upon addition of different metal ions, only with Cu^{2+}, did sensors (1) and (2) show remarkable fluorescence enhancement due to coordination to a paramagnetic Cu^{2+} centre (Fig. 1A and 2A).

Based on earlier studies[37–39] and our own observation we propose the following mechanism. Cu^{2+} is a well–known paramagnetic ion with an unfilled 'd' shell and could strongly quench the fluorescence of the fluorophore near it via electron or energy transfer. Thus it is of interest to us that the Cu^{2+} by compounds (1) and (2) does not quench the fluorescence. It is known that the nitrogen lone pair electrons of compounds (1) and (2) can quench the fluorescence of the indene 1,3-dione moiety through photo induced electron transfer (PET)[40-44]. Masking of the nitrogen lone pair electrons cause a suppression of their fluorescence quenching and therefore, results increase in fluorescence intensity. It is evident from the emission spectra that in the absence of Cu^{2+} the sensor exhibited weak fluorescence owing to the quenching of compounds (1) and (2) fluorescence through PET. And also in the presence of the quenching metal ions, the relative contribution of two opposing factors, the metal-ion receptor binding that leads to enhancement of the fluorescence signal and the fluorophore-metal ion interaction that leads to fluorophore quenching determines the net effect. Therefore possible to observe fluorescence enhancement in the presence of quenching ions when metal binding-induced enhancement of fluorescence intensity is greater, than the quenching- induced reduction in the fluorescence intensity. So, it is clear that for an already PET Quenched system, otherwise

strongly quenching metal ion acts as a poor quencher. Obviously, in the absence of quenching interaction, metal ion binding with receptor will only lead to fluorescence enhancement. Finally we conclude that unavailability of the lone pair electrons of 'N' for PET caused fluorescence enhancement.

The emission at around 500 nm in (1) and 510 nm in (2) did not change when the concentration of Cu^{2+} increased from 1 μmol/L compound **(1)** and **(2)** in 1:1(volume ratio) CH_3CH_2OH/H_2O (10 mmol/L 10 μM HEPES buffer, pH=7.0) binding to Cu^{2+} with different concentrations ion. It implying a 1:1 complexation of compounds (**1**) and (**2**) with Cu^{2+} ions (Fig. 1B and 2B). .The maximum fluorescence enhancement was observed in the presence of 2 μm **(1)** and 1.8 μm in **(2)**. When the concentration of Cu^{2+} was less or equal to around 2 μm, the binding of Cu^{2+} made the polarization of the molecule larger, and it allowed only partial electron transfer, therefore the fluorescence intensity was enhanced but the emission maximum did not change with the increase of Cu^{2+} concentration; whilst the concentration of Cu^{2+} was more than 2 μm, excess Cu^{2+} resulted in a sudden drop of relative intensity was observed, without question due to concentration quenching[45].

Furthermore, the relationship of fluorescence enhancement ratio(defined as I/I_0, where I and I_0 are the fluorescence intensities of compound **(1)** and **(2)** in solution when binding with and without Cu^{2+}, respectively) with the binding concentration of Cu^{2+} was also investigated. Apparently, the ratio was nearly proportional to the molar binding concentration of Cu^{2+} ($R2=$ 0.9941 **(1)** and $R2=0.9986$ **(2)**) when the binding concentration of copper was in a range of 0—5.0 μmol/L (Fig.1c and 2c).

pH-Dependent Behavior

The influence of pH on chemosensor of compounds (**1**) and (**2**) were studied using UV-vis-spectrocopy (Fig. S11). Over a pH range of 3-8, the visible absorption band centered at 480 nm in (**1**) and 450 nm in (**2**) were unchanged. But increase in pH from 9 to 11 engendered a shift in the maximum absorption wavelength to 375 nm (**1**) and 380 nm (**2**) with color change of yellow to blue. This difference were due to the dissociation of (**1**)-Cu^{2+} and (**2**)-Cu^{2+} complex, which result in lower absorbance and color change from yellow to blue.

The pH emission spectra of sensors (**1**) and (**2**) and its ability to detect the Cu^{2+} cations might be influenced by the pH of the solution because of the nitrogen atom of hydrazone moiety with lone pair electrons in the sensors (**1**) and (**2**) .To verify this hypothesis, the pH effect on the fluorescence intensity of sensors (**1**) and (**2**) in the unbound and bound of Cu^{2+} was studied. As shown in Fig. S12, in the unbound of Cu^{2+} (curve b), sensors (**1**) and (**2**) presents a low fluorescence intensity which remain stable and did not change with the pH. Upon addition of Cu^{2+} (curve a), the emission intensity of compounds (**1**) and (**2**) with Cu^{2+} increased dramatically from pH 3 to 5, resulting from the competition between the N-H proton and Cu^{2+} ion[46, 47]. In particular, slight significant change in fluorescence spectra were observed in the range of pH 5-8 and decresed under alkaline condition with a color change of yellow to blue .The quenching at higher pH could be well explained by the formation of $Cu(OH)^-$ or $Cu(OH)_2$ and thus reducing the concentration of Cu^{2+}- (**1**) / (**2**)[48] and therefore there are fewer ions as Cu^{2+} in solution that are able to be complexed with compounds (**1**) and (**2**) which explains the decrease of the fluorescence intensity. The results demonstrate that sensors (**1**) and (**2**) could be used in the environment where the pH ranges from 5 to 8, which covers the physiological pH conditions.

To prove the presence of C, O, N and Cu in the surface of the complexes (corresponds to compound (1) and (2)) using Elemental mapping of FE-SEM was carried out. Fig. 3a and Fig. 4a are exhibits FE-SEM color images of complexes (Compound (1)-Cu^{2+} and (2)-Cu^{2+}), Fig. 3b–e and 4b-e shows the elemental mapping for carbon, nitrogen, oxygen and copper respectively. It is evident from that the Fig. 3b–d and 4b–d, carbon, nitrogen and oxygen are higher in density. There is a homogenous distribution of carbon, nitrogen, oxygen and copper (Fig. 3a and 4a). Thus elemental mapping shows that the complex of compound (1) and (2) contains Cu^{2+}. This also indicates the purity of the complexes (compound (1)-Cu^{2+} and (2)-Cu^{2+}). EDS is generally accurate up to trace amount of metal present in the surface of complexes. The EDS recorded from the selected area is shown in Fig. 3f and 4f, which reveals the presence of C, O, N and Cu in the complexes.

Docking Studies

Molecular docking technique is an eye-catching scaffold to understand between the ligand and protein interactions. We have studied various cancer proteins like 4LRH, 4L9K, 4EKD and 4GIW from Protein data bank. Along with these proteins only 4LRH cancer protein shows good results while compared to other binding energy values. Molecular docking simulation was employed to predict interaction of compound (1) and (2) into 4LRH. We docked compound (1) and (2) with 4LRH as shown in Fig. 5 and 6. The value of free energy binding (ΔE) and binding constant (ki) of compound (1) and (2) are given in table 1. The molecular docking simulation shows that compound (1) has less activity compared with compound (2). The above conclusion is proved from the hydrogen bond formations. The simulations for compound (1) and (2) were carried out with other three cancer proteins (4L9K, 4EKD and 4GIW) as shown in Figs. S17-S22 respectively. From the figures it is evident that 4LRH docks strongly with

compound **(1)** and **(2)**. As shown in figures hydrogen bond distance between compound **(2)** and important residue was smaller than hydrogen bond distance between compound **(1)** and residues. In addition, hydrophobic interaction of compound **(2)**- 4LRH was more strongly than compound **(1)**- 4LRH. The docked pose displayed in Fig. 5a, 5b, 6a and 6b reveals the subdomain IB of the protein to be the favorable binding site for the drug. The principal hydrophobic binding sites in 4LRH are located in domains II and III, while domain I, characterized by a net negative charge, normally serves as an suitable binding site for cationic probe molecules. The lowest binding energy conformer was obtained from 4 different conformers for every docking simulation and the consequential minimum energy conformation was used for further analysis. As is usual in a blind docking simulation protocol, we obtained a number of binding sites and the corresponding binding constants and free energies. Compelling evidence for the probable-binding location of the drug in subdomain IB of 4LRH was derived from the observation that the binding of compounds **(1)** and **(2)** in the IB region was found to be characterized by a favorable binding energy of $-$ 8.25 kcal mol^{-1} and $-$ 8.29 kcal mol^{-1} respectively (Table 1), a very low inhibition constant (900.66 nM) for Compound **(1)** and (837.70 nM) for Compound **(2)**. Fig. 5c marks the protein residues in the near vicinity (within 4 Å) of the probe, which shows the presence of both hydrophobic residues (TYR-60, TRP-171, and TYR-85), as well as charged/polar residues (TRP-102 (cation-pi), TRP-140 and HIS-135) for compound **(1)** and hydrophobic residues (TRP-171, TYR-85, PHE–62, TRP-140 and TRP-138) as well as charged/polar residues (TYR-60 (cation-pi), HIS-135 (hydrogen bond), ARG-103) for compound **(2)(Fig. 6c)** which evinces the binding phenomenon to be mainly governed by hydrophobic forces with a significant contribution from electrostatic interactions. Asymmetric charge distribution over the molecule because of the presence of heteroatoms might have been responsible for such type of binding. Based on

molecular docking results, we conclude that alkyl group has been more responsible into biological activity than aromatic ring.

Cytotoxicity

The cytotoxicity responses of compound **(1)** and **(2)** with various concentrations added are clearly evident from the cellular imaging. Hence, these results indicate that compound **(1)** and **(2)** is an efficient candidate for monitoring changes in the intracellular concentration under certain biological conditions; in order to test its cytotoxicity, we performed MTT assay in KB cancer cells treated with various concentrations of compound **(1)** and **(2)** for up to 5 h. As shown in Figs. 7 and 8, Compounds **(1)** and **(2)** did show significant cytotoxic effects on KB cancer cells for at least up to 4 h. The synthesized compound **(1)** and **(2)** were examined for their cytotoxic properties on KB cell line by means of MTT test that allows us to evaluate the toxic effect of above compounds on cellular mitochondrial metabolism. Cells were tested for 48 h with increasing concentrations of tested compounds. Microscopic images of control cancer cells and apoptotic morphological changes in KB cell line treated with compound **(1)** and **(2)** are shown in Fig. 7 and 8 respectively. The results indicate that the compound **(1)** showed minimum cell death when compared to compound **(2)**. The compounds **(1)** and **(2)** exhibit broad inhibition on the KB cell lines with IC50 values of 32.78 and 40.08 respectively. The IC50 values of the compound (Fig. S23) suggest that compound **(2)** possessed more potent inhibitory effect against the cancer cells. Compound **(2)** carrying the $-OCH_3$ group in para position and shows the highest IC50 value, convincing us to propose that the electronic effect may be one of the factors in determining the anticancer activities of compound **(2)**.[49, 50]

RSC Advances Accepted Manuscript

Theoretical calculations

The geometries of the sensor compound (**1**) and compound (**2**) with Cu^{2+} ion were optimized using DFT-B3LYP 6-31 G and LANL2DZ (d) levels respectively using Gaussian 03 package. In Fig. S24 and S25 the optimized geometries of compound (**1**), compound (**2**) and its 1 : 1 complex with Cu^{2+} ion are given, which displays the effective binding sites, namely –NH and C=O for Cu^{2+} ion. To get an insight into the electronic behavior in the presence and absence of Cu^{2+} with compound (**1**) and compound (**2**), TD-DFT calculations were carried out using the same level. Plotting of HOMO and LUMO of compound (**2**) that the π-electrons on the HOMO of ligand focused on one of the ketone group of dione moity and lumo of the ligand focused on N-NH group of hydrazone moiety. When Cu^{2+} is added, it shows a significant change in the distribution of the π-electrons on HOMO and LUMO. More significantly,the HOMO and LUMO densities in compound (**1**) and (**2**) **with** Cu^{2+} are delocalized over the whole molecule except phenyl ring of dione moiety in HOMO and methoxy phenyl ring in LUMO. The energies of HOMO and LUMO of compound(1) and compound (2)-Cu^{2+} complex are slightly lower than that of compound(1) and compound (2). More importantly, the decreasing energy in the LUMO is more obviously than that of the HOMO. It suggests a smaller HOMO-LUMO gap and a bathochromic shift compared with compounds in emission which may result from the increase of conjugation of the complex.

Conclusion

In summary, the hydrazones of indene-1,3-dione have been synthesized and characterized IR, ^{1}H, ^{13}C NMR spectra studies. The FT-IR, NMR, a promising analytical approach for detecting Cu^{2+} in ethanol : water solutions. When copper ion was added in (**1**) and (**2**) their morphology changes were observed. We have prepared a simple type of fluorescent "turn–on" chemosensor based on

hydrazones shows interesting properties such as high sensitivity for Cu^{2+}. It possesses a high affinity and selectivity for Copper ions relative to most other competitive metal ions by enhancement of the monomer fluorescence emission of hydrazones in organic aqueous solution. We expect that the present design strategy and the remarkable photophysical properties of this sensor will help to extend applications of fluorescent sensors for metal ions. Compounds **(1)** and **(2)** docking with 4LRH, 4L9K, 4EKD and 4GIW proteins only 4LRH cancer protein shows good results while compared to other proteins binding energy values. Compound (1) and (2) has potent invitro cytotoxic against KB cell line. In this present investigation molecular structure, HOMO, LUMO, Mulliken charges and MEP analysis have been studied using ab initio DFT B3LYP/6-31G calculation.

Acknowledgment

Notes and references

1 K. Dhara, U. C. Saha, A. Dan, M. Manassero, S. Sarkar and P. Chattopadhyay, *Chem. Commun.*, 2010, **46**, 1754.

2 U. C. Saha, B. Chattopadhyay, K. Dhara, S. K. Mandal, S. Sarkar, A. R. Khuda-Bukhsh, M. Mukherjee, M. Helliwell and P. Chattopadhyay, *Inorg. Chem.,* 2011, **50**, 1213.

3 H. H. Harris, I. Pickering and G. N. George, *Science,* 2003, **301**, 1203.

4 P. B. Tchounwou, W. K. Ayensu, N. Ninashvile and D. Sutton, *Environ. Toxicol.,* 2003, **18**, 149.

5 Y. Ronghua, L. Kean, W. Kemin, Z. Fenglin, L. Na and L. Feng, *Anal. Chem.,* 2003, **75**, 612.

6. L. B. Desmonts, D. N. Reinhoudt and M. C. Calama, *Chem. Soc. Rev.,* 2007, **36**, 993.

7. H. H. Wang, L. Xue, Z. J. Fang, G. P. Li and H. Jiang, *New J. Chem.,* 2010, **34**, 1239.

8 (a) R. Kramer, *Angew. Chem., Int. Ed.,* 1998, **37**, 772; (b) K. J. Barnham, C. L. Masters and A. I. Bush, *Nat. Rev. Drug Discovery,* 2004, **3**, 205; (c) E. L. Que, D. W. Domaille and C. J. Chang, *Chem. Rev.,* 2008, **108**, 1517; (d) G. L. Millhauser, *Acc. Chem. Res.,* 2004, **37**, 79; (e) E. Gaggelli, H. Kozlowski and G. Valensin, *Chem. Rev.,* 2006, **106**, 1995; (f) G. Multhaup,

A. Schlicksupp, L. Hess, D. Beher, T. Ruppert, C. L. Masters and K. Beyreuther, *Science*, 1996, **271**, 1406; (g) R. A. Lovstad, *BioMetals,* 2004, **17**, 111.

9 G. F. Nordberg, R. F. M. Herber and L. Alessio, Cadmium in the Human Environment, Oxford University Press, Oxford, UK, 1992.

10 C. N. McFarland, L. I. Bendell-Young, C. Guglielmo and T. D. Williams, *J. Environ. Monit.,* 2002, **4**, 791.

11 H. N. Kim, W. X. Ren, J. S. Kim and J. Yoon, *Chem. Soc. Rev.,* 2012, **41**, 3210.

12. Z. Li, W. Zhao, X. Li, Y. Zhu, C. Liu, L. Wang, M. Yu, L. Wei, M. Tang, and H. Zhang, *Inorg. Chem.*, 2012, **51**, 12444.

13 J. W. Liu, Y. Lu, *J. Am. Chem. Soc.,* 2007, **129**, 9838.

14 K. M. K. Swamy, S. K. Ko, S. K. Kwon, H. N. Lee, C. Mao, J. M. Kim, K. H. Lee, J. Kim, I. Shin and J. Yoon, *Chem. Commun.,* 2008, 5915.

15. A. Sigel, H. Sigel, R. K. O. Sigel, Nickel and Its Surprising Impact in Nature; Eds.; Metal Ions in Life Sciences, **2**; Wiley: Chichester, U.K., 2007.

16 (a) A. Banerjee, A. Sahana, S. Guha, S. Lohar, I. Hauli, S. K. Mukhopadhyay, J. Matalobos and D. Das, *Inorg. Chem.*, 2012, **51**, 5699; (b) G. Li, H. Fang, Y. Cai, Z. Zhou, P. K. Thallapally and J. Tian, *Inorg. Chem.*, 2010, **49**, 7241; (c) S. C. Dodani, Q. He and C. J. Chang, *J. Am. Chem. Soc.*, 2009, **131**, 18020.

17 (*a*) A. N. Anthemidis and C. P. Karapatouchas, *Microchim. Acta*, 2008, **160**, 455; (*b*) G. Kaya and M. Yaman, *Talanta*, 2008, **75**, 1127.

18 A. C. Davis, C. P. Calloway Jr and B. T. Jones, *Talanta*, 2007, **71**, 1144.

19 (*a*) X. C. Wang, S. H. Drew,K. J. Lee, J. K. Senecal and L. A. Samuelson, *Nano Lett.*, 2002, **2**, 1273; (*b*) R. Metivier, I. Leray and B. Valeur, *Chem. Eur. J.*, 2004, **10**, 4480.

20 H. Tian, B. Li, J. Zhu, H. Wang, Y. Li, J. Xu, J. Wang, W. Wang, Z. Sun, W. Liu, X. Huang, X. Yan, Q. Wang, X. Yao and Y. Tang, *Dalton Trans.,* 2012, **41**, 2060.

21 Y. Zhao, X. B. Zhang, Z. X. Han, L. Qiao, C. Y. Li, L. X. Jian, G. L. Shen, and R. Q. Yu, *Anal. Chem.,* 2009**, 81***,* 7022.

22 H. H. Wang, L. Xue, Z. J. Fang, Gu. P. Li and H. Jiang, *New J. Chem.,* 2010, **34**, 1239.

23 F. J. Huo, C. X. Yin, Y. T. Yang, J. Su, J. B. Chao and D. S. Liu, *Anal. Chem.,* 2012, 84, 2219.

24 V. Chandrasekhar, S. Das, R. Yadav, S. Hossain, R. Parihar, G. Subramaniam, and P. Sen, *Inorg. Chem.,* 2012, **51**, 8664.

25 Z. Li, W. Zhao, X. Li, Y. Zhu, C. Liu, L. Wang, M. Yu, L. Wei, M. Tang, and H. Zhang, *Inorg. Chem.,* 2012, **51**, 12444.

26 T. Mistri, R. Alam, M. Dolai, S. K. Mandal, A. R. K. Bukhsh and M. Ali, *Org. Biomol. Chem.,* 2013, **11**, 1563.

27 J. T. Yeh, W. C. Chen, S. R. Liu and S. P. Wu, *New J. Chem.,* 2014, **38**, 4434.

28 S. Anbu, R. Ravishankaran, M. F. C. Guedes da Silva, A. A. A. Karande, and Ar. J. L. Pombeiro, *Inorg. Chem.,* 2014, **53**, 6655.

29 F. R. Pavan, P. I. S. Maia, S. R. A. Leite, V. M. Deflon, A. A. Batista, D. N. Sato, S. G. Franzblau and C. Q. F. Leite, *Eur. J. Med. Chem.,* 2010, **45,** 1898.

30 G. Gilli and P. Gilli, The Nature of the Hydrogen Bond: Outline of a Comprehensive Hydrogen Bond Theory, Oxford University Press, Oxford, 2009.

31 J. R. Heldt, J. Heldt, M. Jozefowicz and J. Kaminski, *J. Fluoresc.,* 2001, **11**, 65.

32 L. A. Estrada, J. E. Yarnell and D. C. Neckers, *J. Phys. Chem. A* 2011, **115**, 6366.

33 P.Ashokekumar, V. Thiagarajan, S. Vasanthi and P. Ramamurthy, *J. Photochem. Photobiol., A* 2009, **208**,117.

34 J.R. Lakowicz, Principles of Fluorescence Spectroscopy, second ed., Kluwer Academic/ Plenum Publishers, New York, 1999.

35 M.W.Wong, M.J. Frisch, K.B. Wiberg, J. Am. Chem. Soc. 113 (1991) 4776.

36 P. Gilli and G. Gilli, *J. Mol. Struct.*, 2010, **972**, 2.

37 A. P. de silva, H. Q. N. Gunaratne, T. Gunnlaugsson, A. J. M. Huxley, C. P. McCoy, J. T. Rademacher, and T. E. Rice, *Chem. Rev.*, 1997, **97**, 1515.

38 A. P. de silva, T. S. Moody and G. D. Wright, *Analyst,* 2009, **134**, 2385.

39 A. P. de silva, A. Goligher, H.Q. N. Gunaratne, and T. E. Rice, *Arkivoc* 2003, **8**, 229.

40 Z. Xu, J. Yoon and D. R. Spring, *Chem.commun.,* 2010, **46**, 2563.

41 Z. Xu, Y. Xiao, X. Qian, J. cui, and D. Cui, *Org. Lett.,* 2005, **7**, 889.

42 W. Wang, G. Sprigsteen, S. Gao and B. Wang, *Chem. Commun.,* 2000, 1283.

43 B. Ramachandram and A.Samanta, *Chem.Commun.,* 1997, 1037.

44 B. Ramachandram and B.Samanta, *J. phy. chem. A* 1998, **102**, 10579.

45 K. T. Mahmudov, A. M. Maharramov, R. A. Aliyeva, F. M. Chyragov , R. K. Askerov , P. Q. Hasanov , M. N. Kopylovich and A. J. L. Pombeiro, *J. Mol. Struct.*, 2011, **1006** , 576.

46 L. Xue, G. P. Li, D. J. Zhu, Q. Liu and H. Jiang, *Inorg. Chem.,* 2012, **51**, 10842.

47 Y. Zhang, X. F. Guo, W. X. Si, L. H. Jia and X. H. Qian, *Org. Lett.,* 2008, **10**, 473.

48 X. Y. Zhou, B. R. Yu, Y. L. Guo, X. L. Tang, H. H. Zhang and W. S. Liu, *Inorg. Chem.,* 2010, **49**, 4002.

49 (a) Z. Dai and J. W. Canary, New J. Chem., 2007, 31, 1708–1718; (b) B. Valeur and I. Leray, *Coord. Chem. Rev.,* 2000, **205**, 3.

50 M. Guerrero, J. Pons, J. Ros, M. F. Bardia, O. Vallcorba, J. Rius, V. Branchadell and A. Merkoci, *CrystEngComm.,* 2011, **13**, 6457.

Figure captions and figures

Fig. 1(A) Fluorescence emission spectra of chemosensors for compound **(1)** (1μmol/L) with different metal ions (perchlorate, chloride, or nitrate salts of (a) Cu^{2+}, (b) Ni^{2+}, (c) Co^{2+}, (d) Zn^{2+}, (e) Pb^{2+}, (f) Hg^{2+}, (g) Mg^{2+}, (h) Cr^{3+}, (i) Na^+, (j) K^+, (k) Fe^{2+}, (l) Fe^{3+}, (m) Al^{3+}, (n) Cd^{2+} and (o) Ag+) in aq CH_3CH_2OH (CH_3CH_2OH/H_2O = 1:1, v/v, 10 μM HEPES buffer, pH = 7.0), (B) Emission spectra of compound (1) in the presence of an increasing Cu^{2+} concentration Cu^{2+} /(μmol L^{-1}) from a to o 0, 0.2, 0.6, 0.8, 1.0, 1.2, 1.4, 1.2, 1.4, 1.6, 1.8, 2, 2.5, 3.5, 4.0, 4.5, 5.5 1 μmol/L compound **(1)** in 1:1(volume ratio) CH_3CH_2OH/H_2O (10 mmol/L 10 μM HEPES buffer, pH=7.0) binding to Cu^{2+} with different concentrations.(c) Fluorescence enhancement relationship of I/I_0 with $[Cu^{2+}]/[compound(1)]$.

Fig. 2 (A) Fluorescence emission spectra of 10μm solutions chemosensors for compound (2) with different metal ions (perchlorate, chloride, or nitrate salts of (a) Cu^{2+}, (b) Ni^{2+}, (c) Co^{2+}, (d) Zn^{2+}, (e) Pb^{2+}, (f) Hg^{2+}, (g) Mg^{2+}, (h) Cr^{3+}, (i) Na^+, (j) K^+, (k) Fe^{2+}, (l) Fe^{3+}, (m) Al^{3+}, (n) Cd^{2+} and (o) Ag+) in aq CH_3CH_2OH (CH_3CH_2OH/H_2O = 4/1, v/v, 10 μM HEPES buffer, pH = 7.0), (B) Emission spectra of compound (2) in the presence of an increasing Cu^{2+} concentration Cu^{2+} /(μmol L^{-1}) from a to o 0, 0.2, 0.6, 0.8, 1.0, 1.2, 1.4, 1.2, 1.4, 1.6, 1.8, 2, 2.5, 3.5, 4.0, 4.5, 5.5 1 μmol/L compound **(2)** in 1:1(volume ratio) CH_3CH_2OH/H_2O (10 mmol/L 10 μM HEPES buffer, pH=7.0) binding to Cu^{2+} with different concentrations ion.(c) Fluorescence enhancement relationship of I/I_0 with $[Cu^{2+}]/[compound(2)]$.

Fig. 3 FE-SEM elemental colour mapping image of compound (1)-Cu^{2+}(a) survey spectrum, (b) C, (c) N (d) O (e) Cu and (f) EDS spectra.

Fig. 4 FE-SEM elemental colour mapping image of compound (2)-Cu^{2+} (a) survey spectrum, (b) C, (c) N, (d) O, (e) Cu and (f) EDS spectra.

Fig. 5 Molecular docking studies of compound **(1)** with 4LRH.

Fig. 6 Molecular docking studies of compound **(2)** with 4LRH.

Fig. 7 Live Cell images of compound **(1)**: (a) before and (b and c) after treatment with Compound (1) examined by fluorescence microscopy.

Fig. 8 Live Cell images of compound **(2)**: (a) before and (b and c) after treatment with Compound (1) examined by fluorescence microscopy.

Fig. 9 Photoinduced Electron Transfer (PET) of compound **(1)** and compound **(2)** with Cu^{2+}.

Scheme 1 Schematic representation of synthesis of Hydrozone.
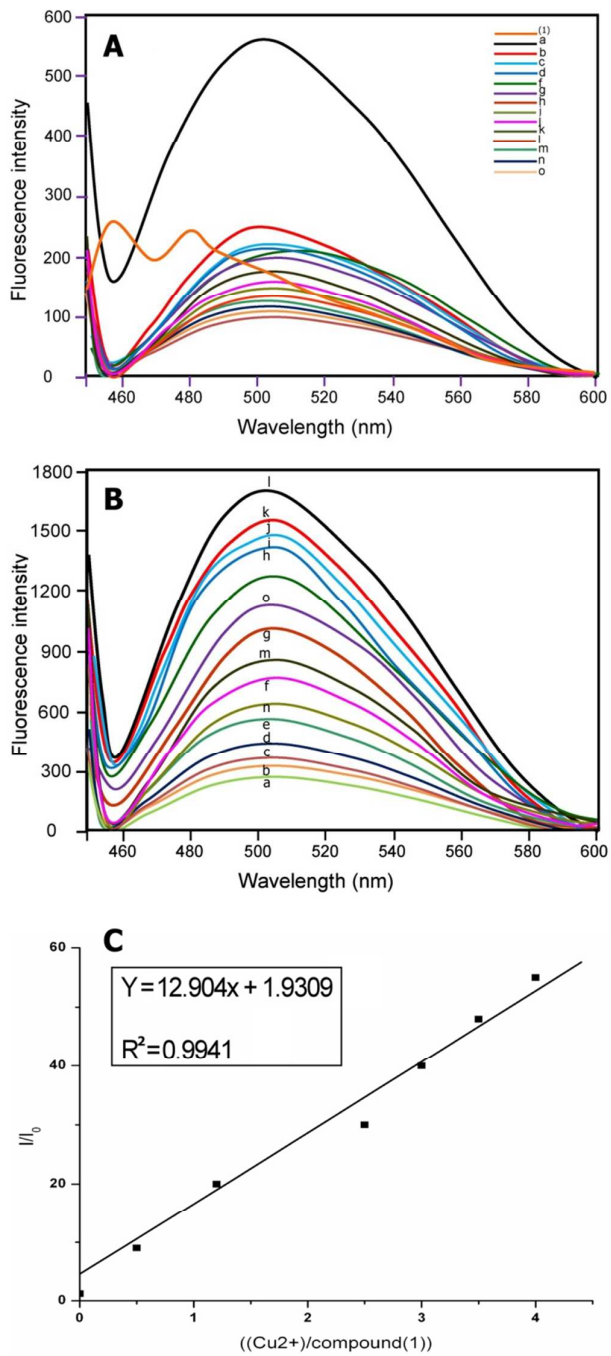
Fig. 1
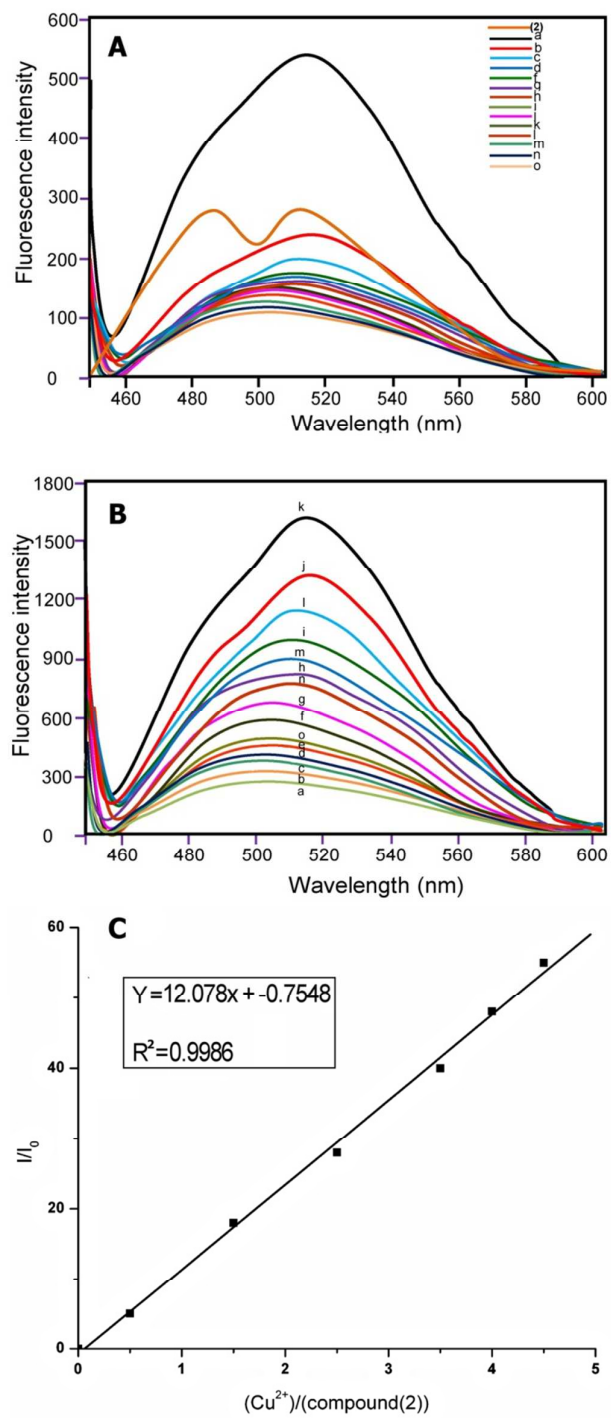
Fig. 2
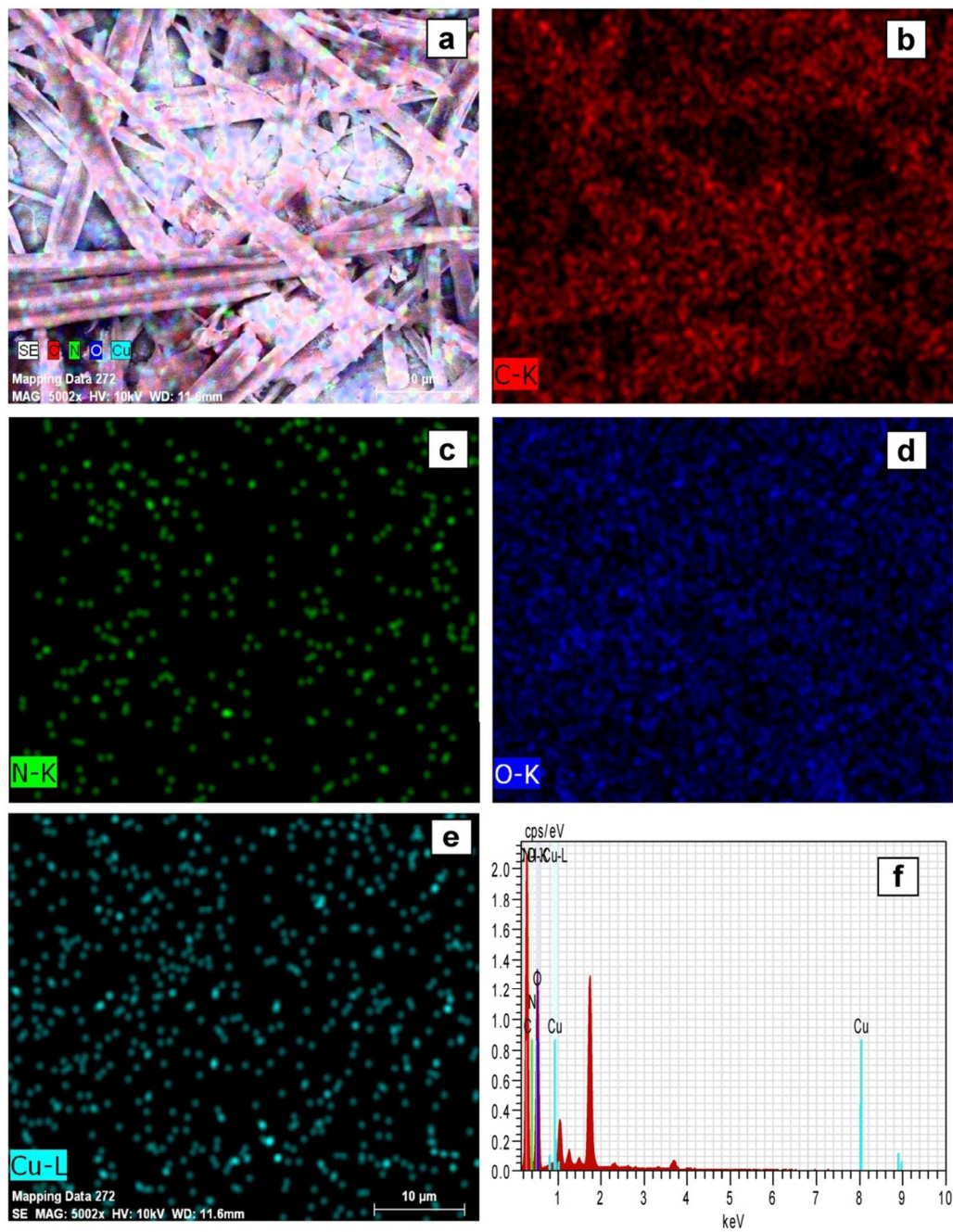
Fig. 3

Fig. 4

Fig. 5

Fig. 6

Fig. 7

Fig. 8

Weakly fluorescent · Strongly fluorescent
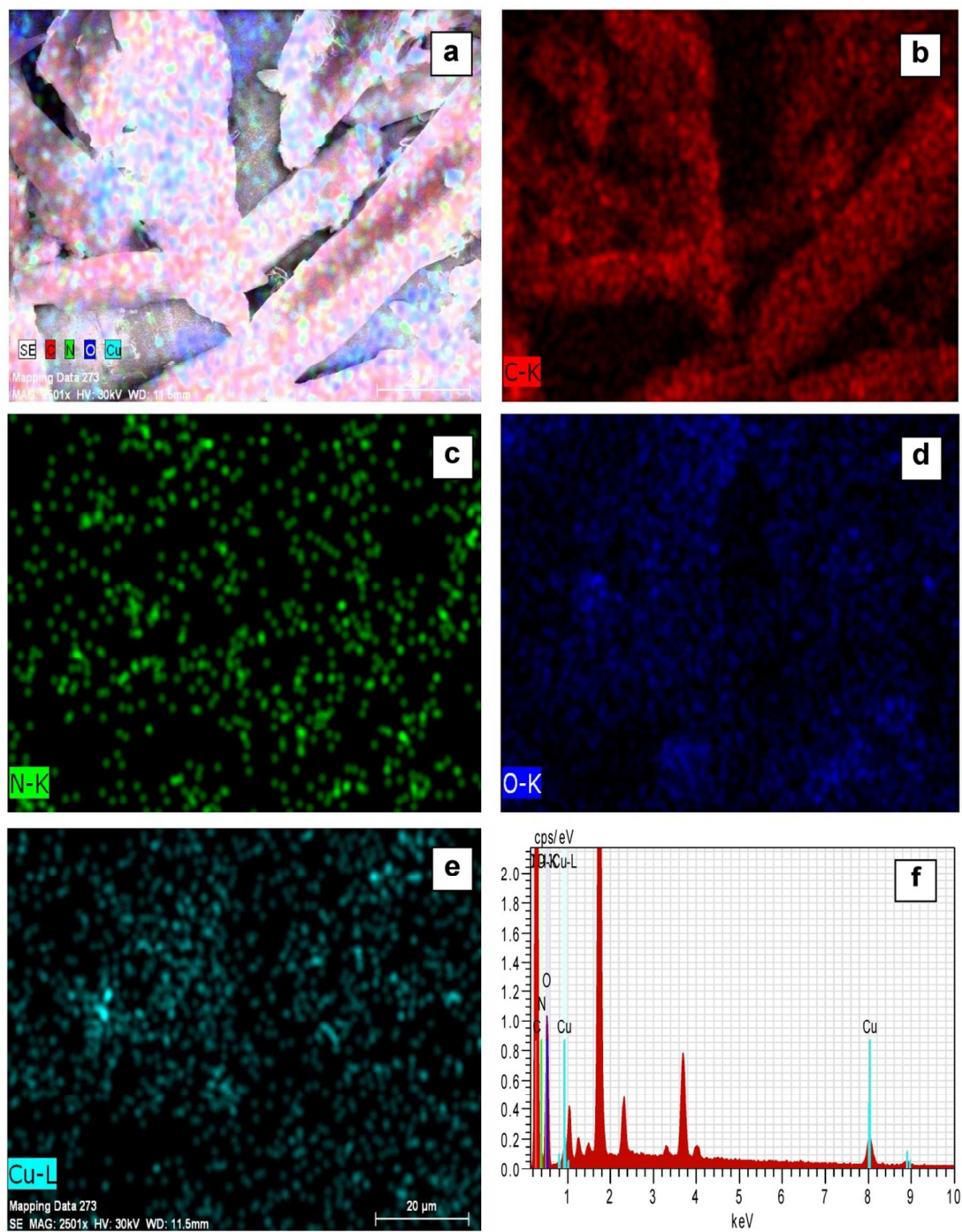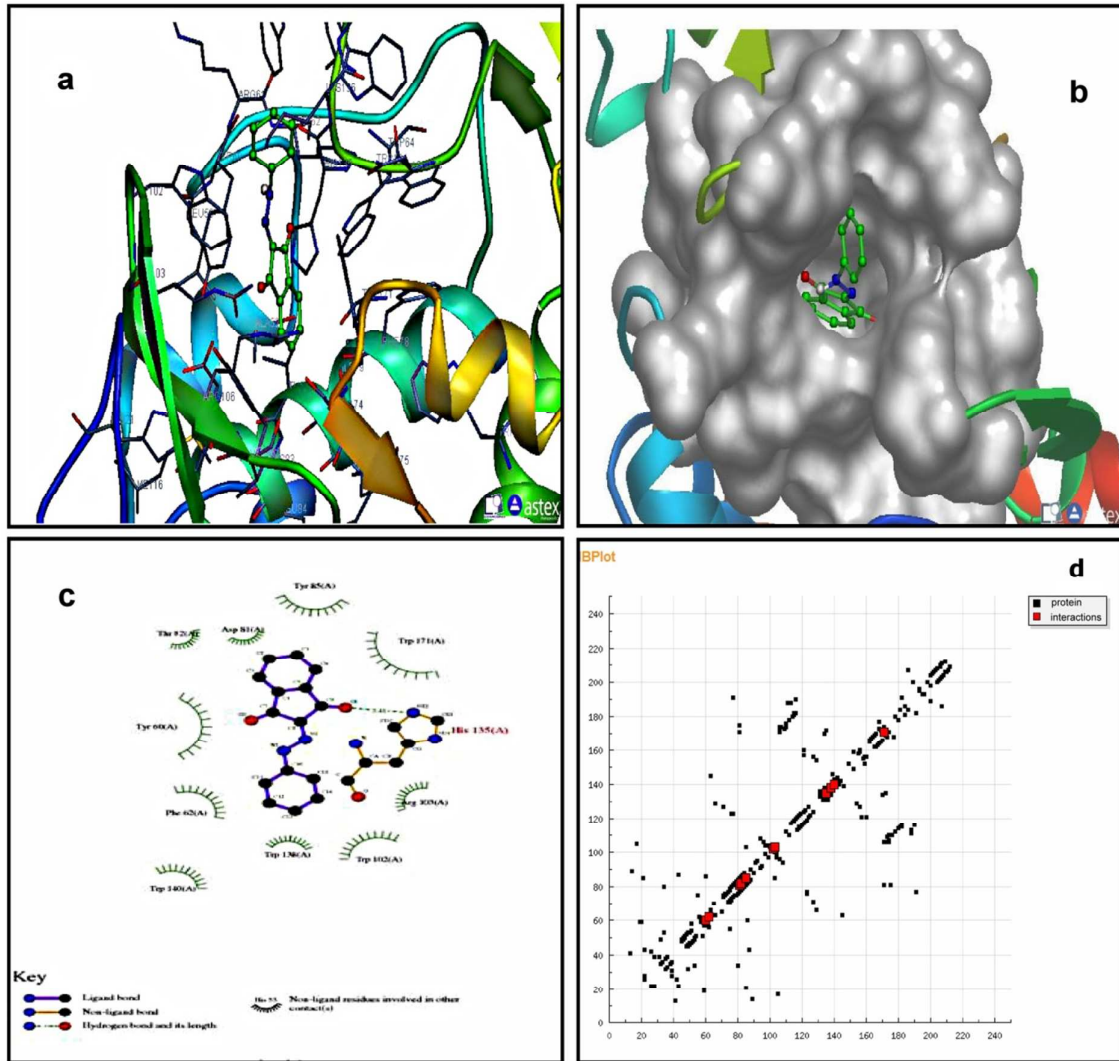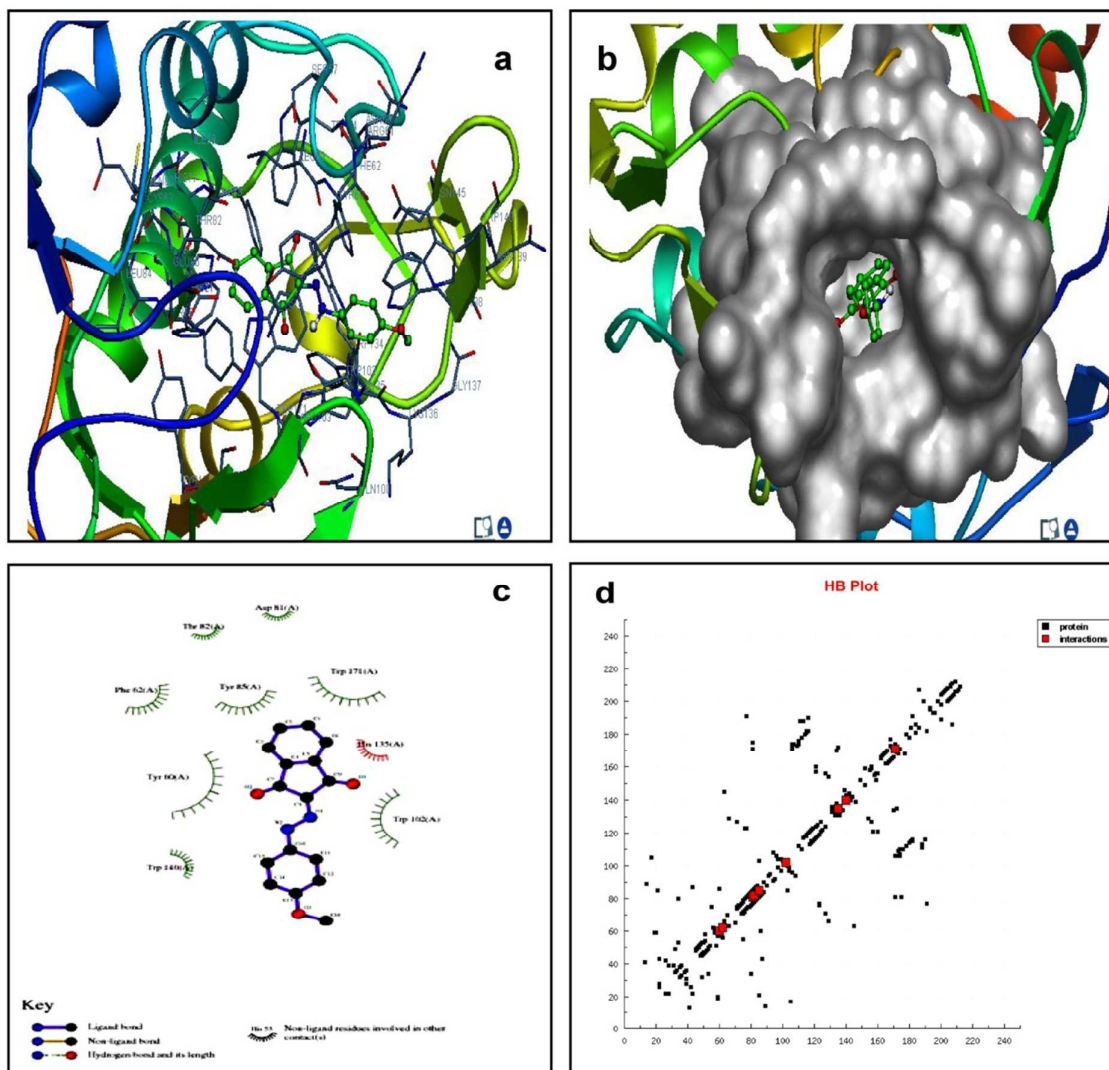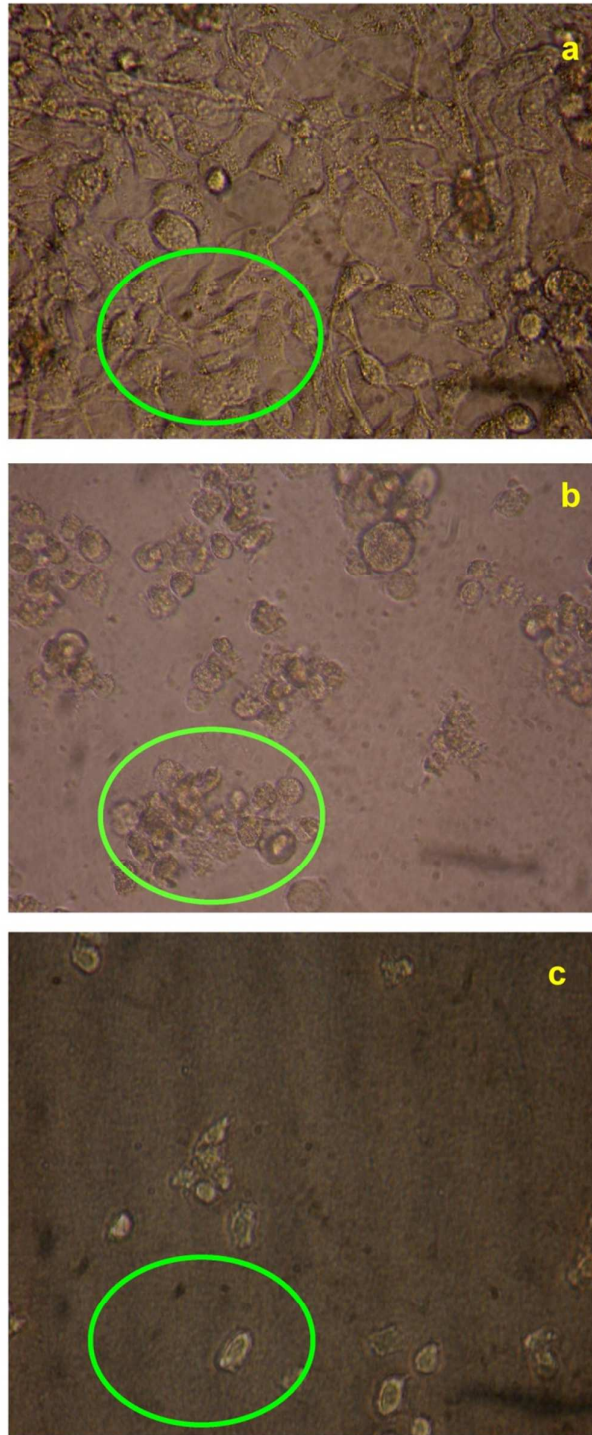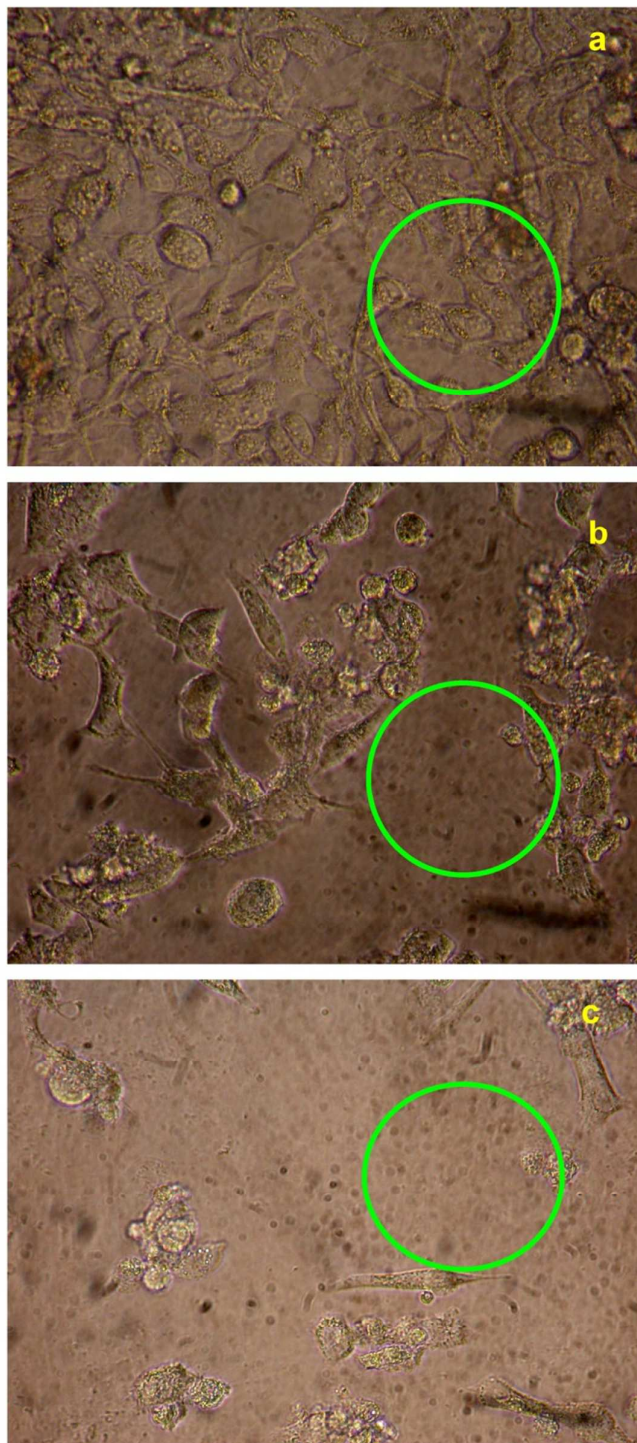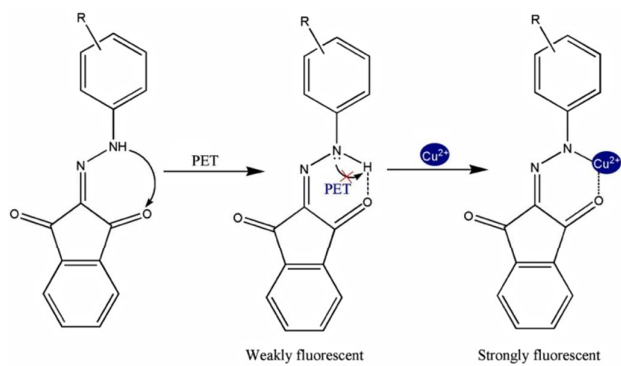
Fig. 9
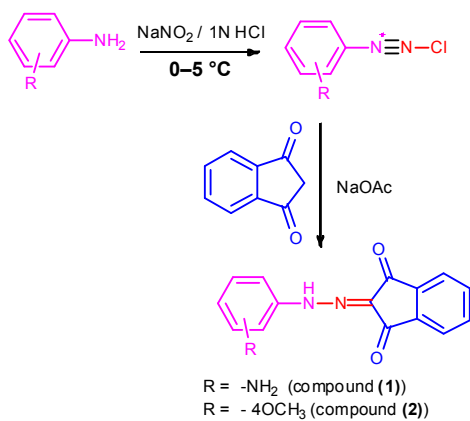
Scheme 1

S.No	Proteins Code	Compound (1)		Compound (2)	
		Free energy of binding (ΔE)	Inhibition constant (Ki)	Free energy of binding	Inhibition constant (Ki)
1	4L9K	-6.97	7.78 uM	-7.32	4.28 uM
2	**4LRH**	**-8.25**	**900.66 nM**	**-8.29**	**837.70 nM**
3	4EKD	-6.96	7.94 uM	-7.24	4.95 uM
4	4GIW	-6.50	17.25 uM	-6.79	10.53 uM

Table 1. Moleulcar docking study of compound **(1)** and **(2)** with different protein and its Free energy of binding (ΔE) and Inhibition constant (Ki) values.

Graphical Abstract
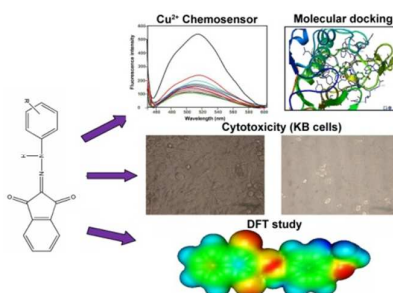
An extremely fluorescent chemosensor based on 2-(2-phenylhydrazono)-1*H*-indene-1,3(2*H*)-dione **(1)** and 2-(2-(4-methoxyphenyl)hydrazono)-1*H*-indene-1,3(2*H*)-dione **(2)** with high sensitivity and selectivity toward Cu^{2+} was developed over other cations. The cytotoxicity study, the ability of these compounds (**1**) and (**2**) to inhibit the growth of KB cell lines.